FR-60291.ADD

Final Technical Report Addendum for:

VISIBLE AND INFRARED (1.54 μm) LED BASED ON ER-DOPED POROUS Si

Submitted under:

Contract No. F49620-93-C-0040

Submitted to:

Administrative Contracting Officer, AFOSR/PKA

110 Duncan Avenue, Suite B115

Bolling AFB, DC 20332-0001

Submitted by:

Spire Corporation

One Patriots Park

Bedford, MA 01730-2396

REPORT DOCUMENTATION PAGE

Form Approved OMB No. 0704-0188

1. AGENCY USE ONLY *(Leave blank)*	2. REPORT DATE	3. REPORT TYPE AND DATES COVERED
	28 February 1994	1 JUL-31 DEC 1993 Draft Final

4. TITLE AND SUBTITLE
Visible and Infrared (1.54 μm) LED Based on Er-doped Porous Si

5. FUNDING NUMBERS
F49620-93-C-0040

6. AUTHOR(S)
Fereydoon Namavar

7. PERFORMING ORGANIZATION NAME(S) AND ADDRESS(ES)
Spire Corporation
One Patriots Park
Bedford, MA 01730-2396

8. PERFORMING ORGANIZATION REPORT NUMBER
AFOSR-TR- 94 0199
FR-60291

9. SPONSORING/MONITORING AGENCY NAME(S) AND ADDRESS(ES)
Administrative Contracting Officer, AFOSR/NE
110 Duncan Avenue, Suite B115
Bolling AFB, DC 20332-0001

10. SPONSORING/MONITORING AGENCY REPORT NUMBER
3005/SS

11. SUPPLEMENTARY NOTES

12a. DISTRIBUTION/AVAILABILITY STATEMENT
Approved for public release
distribution unlimited.
Unlimited

12b. DISTRIBUTION CODE

13. ABSTRACT *(Maximum 200 words)*

Phase I demonstrated strong room-temperature 1.54 μm luminescence from visible light-emitting porous Si doped with erbium. Er was implanted with a dose of $10^{15}/cm^2$ at 190 keV into porous Si, bulk Si, GeSi, quartz, and sapphire . The highest emission intensity was observed for porous Si samples which were annealed at 650°C and had a peak concentration of 1.5×10^{20} Er/cm^3. However, no IR emission was observed from Er in bulk Si, GeSi, quartz, and sapphire. Our results show that the high PL efficiency in Er-implanted porous Si originates from Er confined in < 5nm-diameter Si nanostructures. In these samples, only an insignificant decrease in PL intensity was observed from 77 to 300K.

In addition, Phase I work clearly indicates that photoluminescence (PL) intensity is almost comparable to $In_{0.53}Ga_{0.47}As$ material, which is used for commercial infrared (IR) light-emitting diodes (LEDs). These results suggest that Er:porous-Si electroluminescent devices with practical quantum efficiency at 300K are feasible.

14. SUBJECT TERMS
porous Si, visible light emission, Er implantation, infrared emission, nanostructures photoluminescence, electroluminescence, room temperature, fiber optics

15. NUMBER OF PAGES
24

16. PRICE CODE

17. SECURITY CLASSIFICATION OF REPORT	18. SECURITY CLASSIFICATION OF THIS PAGE	19. SECURITY CLASSIFICATION OF ABSTRACT	20. LIMITATION OF ABSTRACT
Unclassified	Unclassified	Unclassified	Unlimited

 FR-60291.ADD

Final Technical Report Addendum for:

VISIBLE AND INFRARED (1.54 μm) LED BASED ON ER-DOPED POROUS Si

Submitted under:

Contract No. F49620-93-C-0040

Submitted to:

Administrative Contracting Officer, AFOSR/PKA

110 Duncan Avenue, Suite B115

Bolling AFB, DC 20332-0001

Submitted by:

Spire Corporation

One Patriots Park

Bedford, MA 01730-2396

1 FABRICATION OF POROUS Si:Er DIODES

1.1 Device structures for visible and IR LEDs

Extensive efforts have been carried out to fabricate and test infrared light-emitting devices based on Er-implanted porous Si. A list of test structures fabricated in Phase I are summarized in Table I. For comparison, test structures were fabricated on bulk Si, Si-on-sapphire, porous Si and Er-doped porous Si.

We initiated our work with the fabrication of heterojunction diodes by depositing a layer of indium-tin-oxide (ITO) through a physical mask onto Er-implanted p-type porous Si samples, using a sputtering technique. The ITO target used for sputtering contained less than 9% Sn, to allow formation of films which would be transparent for both visible and near IR wavelengths. An ohmic contact was made to the non-porous Si substrate on the back side by electron-beam evaporating a layer of aluminum. Al was evaporated through a mask so that IR emission could also be observed from the back side. Figures 1a and 1b show, respectively, a cross sectional schematic and an actual photograph of a sample with ITO on Er-implanted porous Si np-heterojunction structures.

1.2 Device Structures for IR LEDs

A study of simultaneous visible and IR light emission from Er-implanted porous Si is essential for development of visible and IR LEDs. Figure 2 compares luminescence from Er at 1.54 μm and visible light from Si nanostructures versus annealing temperatures. It is clear that an inverse relationship exists between visible and IR emission at 1.54 μm. This figure indicates that strong visible or IR emission can be observed for each annealing condition.

Based on this data, we decided to fabricate structures for IR light-emitting devices using a Au contact. These devices are configured as Schottky diodes between a gold contact and Er-implanted porous Si. Processing for Au Schottky devices is much easier than for ITO heterojunctions. Visible light-emitting Schottky barrier porous Si LEDs have been fabricated by Japanese and German groups, and have been shown to exhibit good electroluminescence. However, the common problem with their devices is that in order to allow visible light emission, the gold layer must be very thin, less than 100Å. Such a problem does not exist for infrared devices, because Si substrates are transparent to IR emission at 1.54 μm and a very thin Au contact is not necessary.

It should be noted that it may be possible that by varying the annealing conditions we may obtain both visible and IR emission simultaneously; we will investigate this in Phase II.

To optimize device structures we used two different methods for depositing Au films on the porous Si layers. As shown in Table I, most samples were Au coated using an RF sputtering machine. We also used an in-house ion beam assisted deposition (IBAD) machine to form the Au contacts. Figure 3 shows a schematic illustration and photographs of porous Si:Er/Au Schottky diodes fabricated by both deposition methods. Structures shown in Figure 3b (sample #SW-32B-Er) were fabricated using RF sputtering while structures shown in Figure 3c (sample #SFPD2-Er) were deposited with Au using IBAD. Note that metal contacts deposited by IBAD typically have better adhesion and are more dense than films deposited by e-beam evaporation or by sputtering.

Table I *List of the samples used for device fabrication in Phase I.*

Sample ID	Substrate Information & Etching Conditions	Implantation Conditions	Annealing in N_2	Deposition of Contact
6554-P	<100> p-type 0.1-1.0 Ωcm 25 mA, 45 min	Er 1E15 380 keV	650°C 30 min	ITO
SW32B-Er	<100> p-type 0.8-1.2 Ωcm 100 mA, 60 min	Er 1E15 190 keV	650°C 30 min	sputter Au
SW32B-Er	<100> p-type 0.8-1.2 Ωcm 100 mA, 60 min	Er 1E15 190 keV	—	sputter Au
SFPD2-Er	<111> p-type 13 Ωcm 100 mA, 45 min	Er 1E15 190 keV	—	sputter Au
control porous Si	p-type 20 mA, 30 min	—	—	sputter Au (transparent)
SW32B-Er	<100> p-type 0.8-1.2 Ωcm 100 mA, 60 min	Er 1E15 190 keV	650°C 30 min	sputter Au (transparent)
SW32B-Er	<100> p-type 0.8-1.2 Ωcm 100 mA, 60 min	Er 1E15 190 keV	—	sputter Au (transparent)
SW32P	<100> p-type 0.8-1.2 Ωcm 10 mA, 60 min	Er 1E15 190 keV	—	sputter Au (transparent)
SFPD2-Er	<111> p-type 13 Ωcm 100 mA, 45 min	Er 1E15 190 keV	—	sputter Au (transparent)
6554-C	<100> p-type 0.1-1.0 Ωcm 100 mA, 60 min	Er 1E15 380 keV	650°C 30 min	sputter Au (transparent)
6554-I	<100> p-type 0.1-1.0 Ωcm 50 mA, 45 min	Er 1E15 380 keV	650°C 30 min	sputter Au (transparent)
6554-F	<100> p-type 0.1-1.0 Ωcm 50 mA, 30 min	Er 1E15 190 keV	650°C 30 min	sputter Au (transparent)
6554-P	<100> p-type 0.1-1.0 Ωcm 25 mA, 45 min	Er 1E15 380 keV	650°C 30 min	sputter Au (transparent)
6554-G	<100> p-type 0.1-1.0 Ωcm 10 mA, 60 min	Er 1E15 380 keV	650°C 30 min	sputter Au (transparent)
SFPD2-Er	<111> p-type 13 Ωcm 100 mA, 45 min	Er 1E15 190 keV	—	IBAD Au

Sample ID	Substrate Information	Implantation Conditions	Annealing in N_2	Deposition of Contact
Si-on-Sapphire	0.4 ± 0.15 μm	Er 1E15 190 keV	—	sputter Au
Si-on-Sapphire	0.4 ± 0.15 μm	Er 1E15 190 keV	—	sputter Au (transparent)
Si-Er	<100> p-type 0.01-0.02 Ωcm	Er 1E15 190 keV	—	sputter Au
Si-Er	<100> p-type 0.01-0.02 Ωcm	Er 1E15 190 keV	—	sputter Au (transparent)
Si-Er	<100> p-type 0.01-0.02 Ωcm	Er 1E15 190 keV	—	IBAD Au

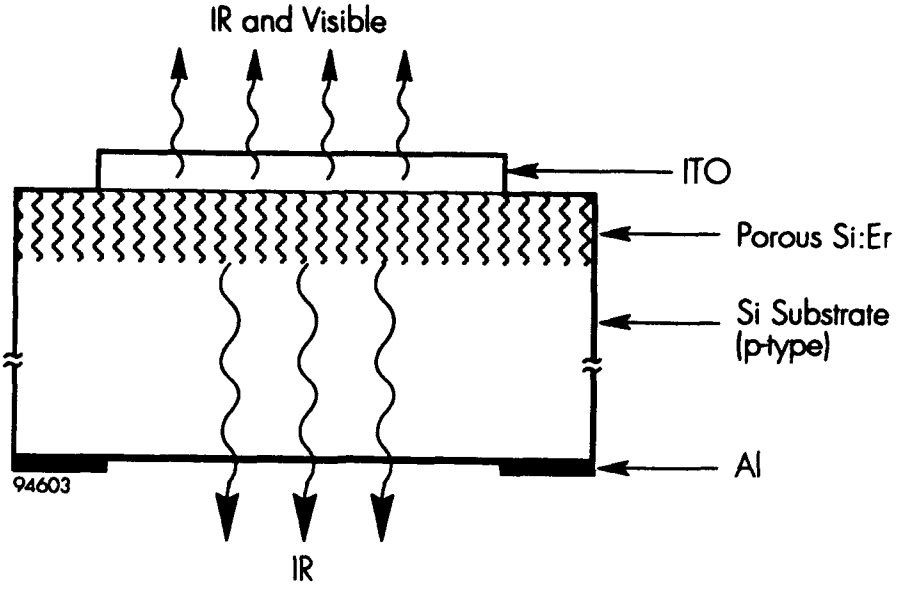

a.)

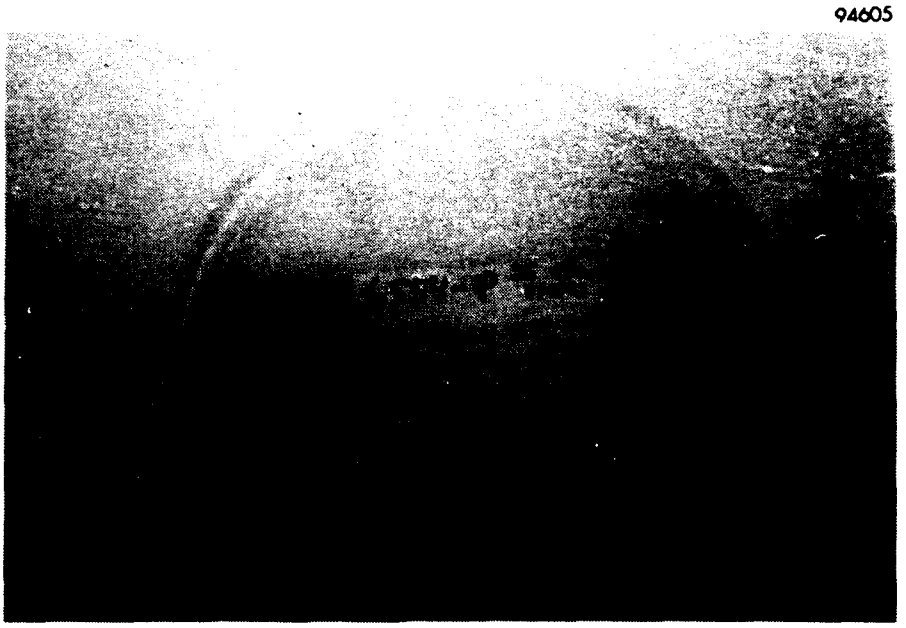

b.)

Figure 1 *ITO Er-implanted porous Si np-heterojunction structures, a) a cross-sectional schematic, and b) an actual photograph.*

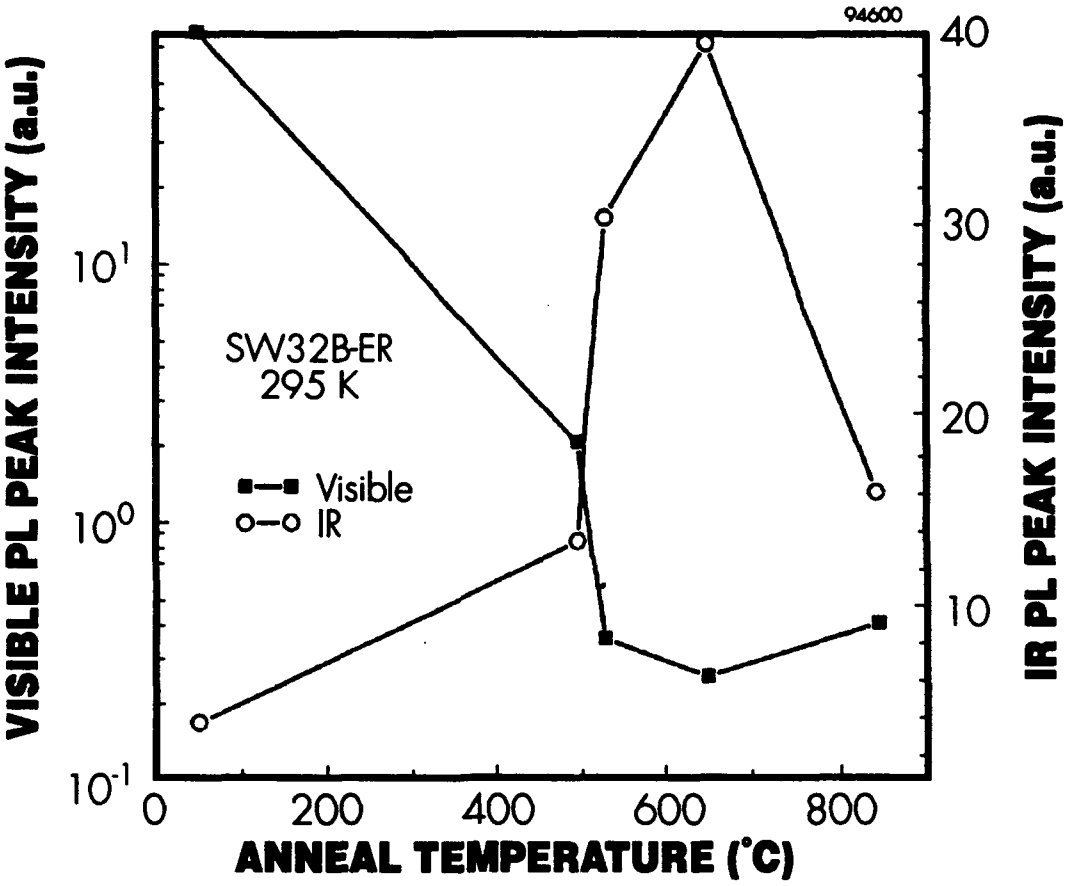

Figure 2 *Intensity of visible and IR emission versus annealing temperature for a porous Si sample implanted with 10^{15} Er/cm^2 at 190 keV.*

a.)

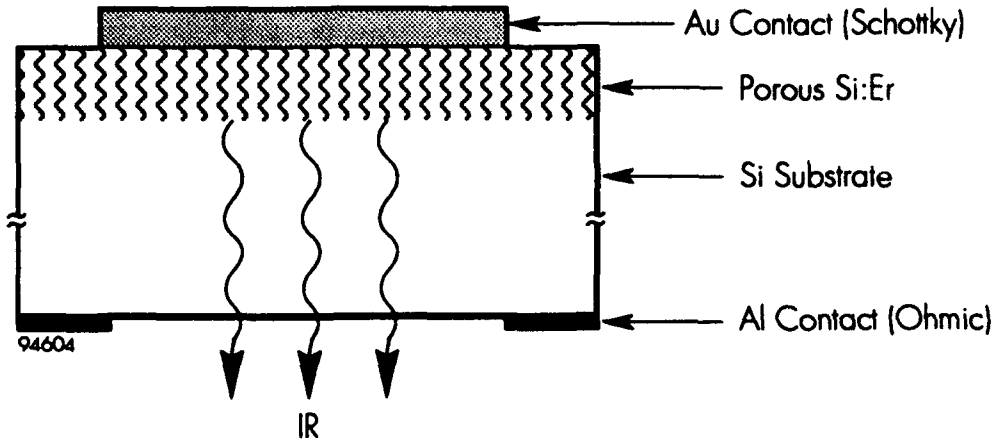

b.)

c.)

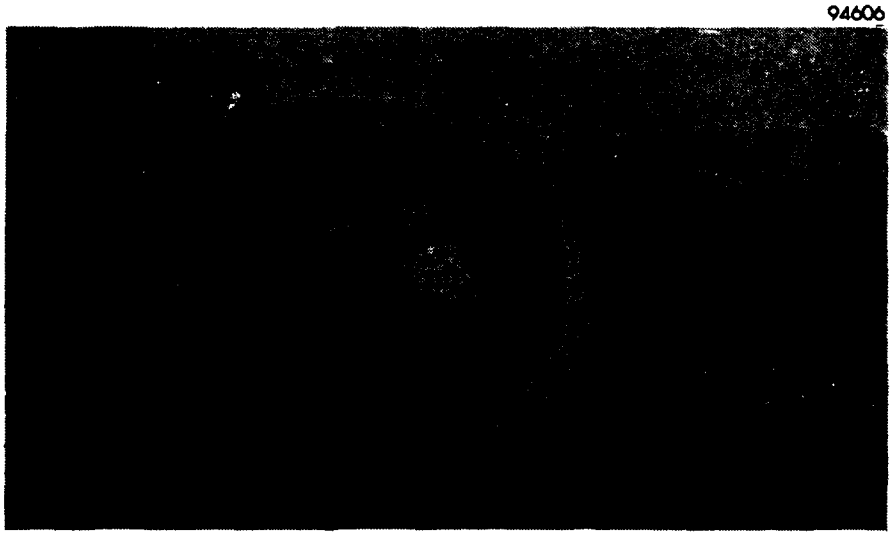

Figure 3 *Er-implanted porous Si/Au Schottky structures; a) Schematic illustration, b) photograph of sample (#SW-32B-Er) with rf-sputtered contacts, and c) photograph of sample (#SFPD2-Er) with IBAD-coated Au contacts.*

As shown in Table I, we fabricated devices on substrates produced under different etching conditions to relate material characteristics to optoelectrical properties. Furthermore, several standard bulk Si and Si-on-Sapphire substrates with and without Er implantation were used as a control. Substrates implanted with 10^{15} Er at 190 and 380 keV were used to compare the effects of implantation energy. All annealing was performed for 30 minutes at 650°C, the temperature at which the maximum PL efficiency was observed.

2 CHARACTERIZATION OF POROUS Si:Er DIODES

2.1 Electrical Characterization

Following the completion of device fabrication, we studied electrical properties of the ITO- and Au-deposited Er-implanted porous Si devices. Using a curve tracer, we tested diode characteristics of each device. Figure 4 shows the current-voltage (I-V) characteristics of an ITO/ porous Si:Er heterojunction diode from sample #6554-P. As shown, the device has typical diode characteristics with excellent rectifying behavior. Figures 5 and 6 show the I-V curves for Au-deposited Er-implanted porous Si Schottky diodes of samples SW32B and SFPD2-Er, which used sputtering and IBAD techniques, respectively.

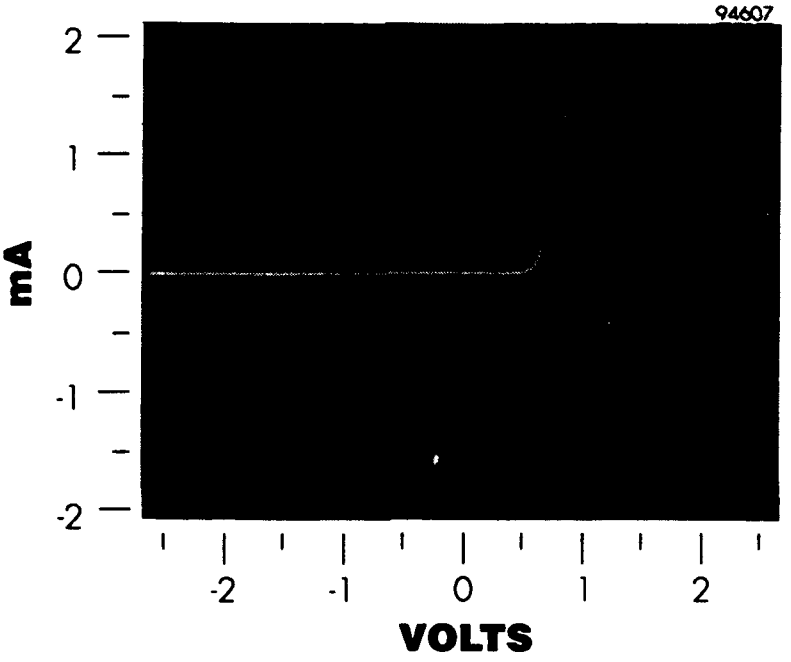

Figure 4 *Current-voltage (I-V) characteristics of an ITO/porous Si:Er heterojunction diode on sample #6554-P.*

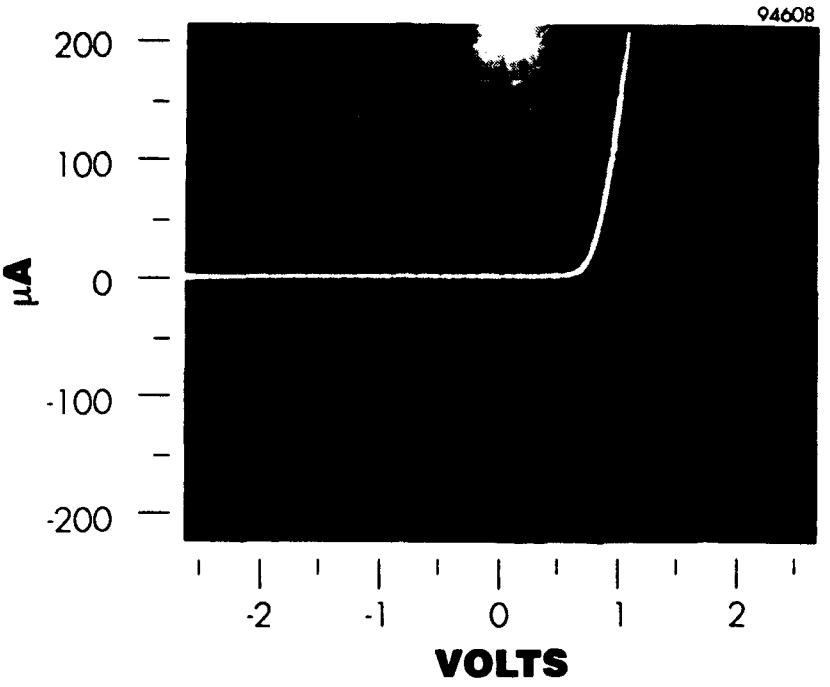

Figure 5 *Current-voltage (I-V) characteristics of an Au/porous Si:Er Schottky diode on sample #SW32B.*

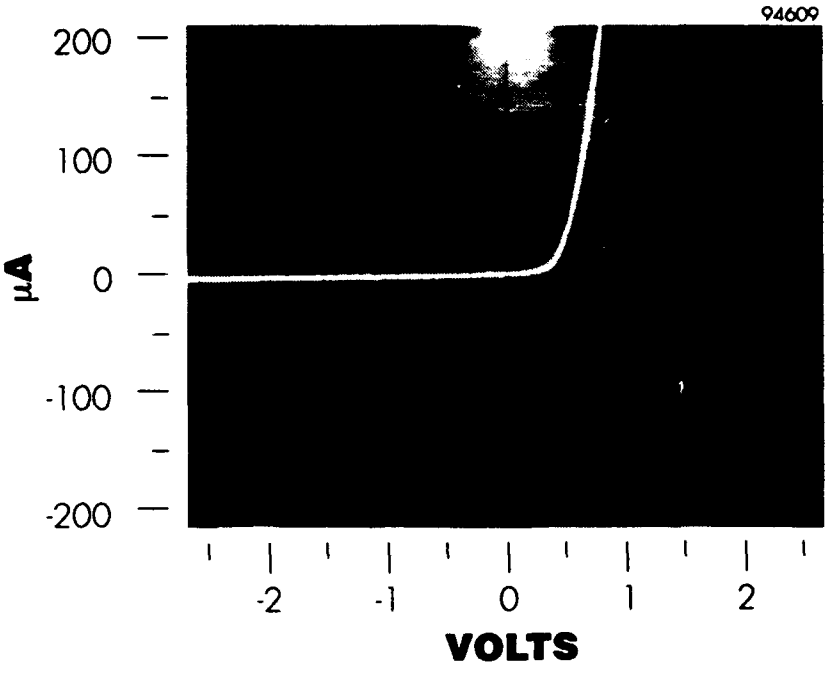

Figure 6 *Current-voltage (I-V) characteristics of an Au/porous Si:Er Schottky diode on sample #SFPD2-Er.*

2.2 Optical Characterization

As mentioned in the final report, infrared spectroscopy for this work was carried out in collaboration with Professor Clive Perry and his post-doctoral fellow Dr. Feng Lu, who was partially supported by this program at Northeastern University. Professor Perry's lab has a NorthCoast Ge detector which provides us with the opportunity to perform these measurements. Spire has a complete facility for study of visible luminescence, which will be expanded in Phase II, to measure infrared emission by purchasing a NorthCoast Ge detector.

Infrared light-emitting devices based on ITO and Au have been provided to Northeastern University for IR luminescence measurements. However, the EL measurements did not materialize because of a new opportunity for Dr. Lu to work at Hanscom AFB. Since Rome Laboratory possesses a NorthCoast Ge detector, we are presently in the process of studying the EL properties of these devices at Hanscom AFB in collaboration with Dr. Lu and Dr. Richard Soref. Results will be reported as they become available.

TABLE OF CONTENTS

LIST OF ILLUSTRATIONS

LIST OF ILLUSTRATIONS (Concluded)

SUMMARY

Phase I demonstrated for the first time strong room-temperature emission at 1.54μm from Er-implanted porous silicon. The photoluminescence (PL) intensity proved to be comparable to that of $In_{0.53}Ga_{0.47}As$ material, which is typically employed in commercial infrared (IR) light-emitting diodes (LEDs) used in fiber telecommunications systems.

Standard InGaAsP IR LEDs find limited use because of their very broad emission spectra, which tend to distort data transmitted in fibers. This distortion of transmitted data is the result of chromatic dispersion, which originates from wavelength dependence on the index of refraction. The problem becomes further amplified because of the dependence of the width of emission spectra of InGaAsP LEDs on operating temperature and power. In contrast, luminescence from rare earth elements such as erbium is narrow and possesses excellent temperature stability because of its inner shell ionic transitions. Porous silicon doped with erbium is a low-cost alternative which can be easily integrated with standard silicon wafer technology.

In this program, erbium was implanted into porous Si, bulk Si, GeSi, quartz, and sapphire at 50 to 400 keV with a dose of $10^{15}/cm^2$. Samples were then annealed for 30 minutes in nitrogen at temperatures ranging from 500°C to 850°C. The highest emission intensity was observed for samples implanted at 190 keV, which had a peak concentration of 1.5×10^{20} Er/cm^3 and were annealed at 650°C. However, no IR emission was observed from Er in bulk Si, GeSi, quartz, and sapphire. These results indicate that strong emission is due to Er in quantum-confined Si nanostructures and not from Er in SiO_2 or in Si with bulk properties. The reduction of PL intensity in Er:porous-Si over the 77 to 300K temperature range is only about two, as compared to the 1000-fold decrease in Er:bulk-Si. These results suggest that Er:porous-Si electroluminescent devices with practical quantum efficiency at 300K are feasible.

We observed strong room-temperature emission by implanting erbium at 190 keV using a simple commercial ion implanter, in contrast to multiple implantation in the MeV range, which has been used by others for introducing erbium into silicon. Note that the cost of implanters, including initial investment and operation, increases exponentially with energy. Therefore, Spire's process provides a very economical and practical approach for fabrication of IR LEDs.

SECTION 1
INTRODUCTION

Through the rapid progress of integrated circuit (IC) technology, silicon has become the leading semiconductor material and will likely remain uncontested for many years; its indirect bandgap, however, has prevented its use in optoelectronics. Extensive research is being conducted in an effort to incorporate compound semiconductor light-emitting diodes (LEDs) and laser diode technologies into silicon very large scale integrated (VLSI) processes by epitaxial growth. However, the most promising III-V light-emitting compounds are not easily processed on silicon substrates due to lattice and thermal expansion mismatches. Incompatibility problems generally degrade the performance of any III-V compound LED grown on silicon. An alternate method involves mounting III-V based devices onto silicon wafers, but this is cost ne-consuming, and labor-intensive.

Two approaches that could overcome this limitation and permit efficient visible to infrared (IR) emission are production of porous Si quantum-confined structures[1] for efficient visible-light emission, and introduction of rare earth elements into Si for IR emission.

During the past two years, optically excited visible-light emission[1] from electrochemically etched anodized silicon[2] has provided researchers with the possibility of fabricating a visible LED based on porous Si.[3-6] A few groups have used semi-transparent Au as a solid state contact to porous Si to form Schottky diodes.[4,5] Spire has demonstrated a light-emitting device consisting of a heterojunction between electrochemically etched p-type porous Si and *n*-type transparent indium tin oxide (ITO) (Figure 1). The use of ITO or other wide-bandgap semiconductors[3,7] which are transparent to visible light has potential applications for visible LEDs and display panels. Extensive efforts are in progress to increase light efficiency in these devices.

Over the last decade, research has focused on the introduction of rare earth elements into III-V compound semiconductors[8-10] because of their potential applications in optical communications. Erbium has attracted the most interest because it exhibits sharp luminescence at 1.54 μm, the result of an internal 4f transition. The 5s and 5p shells shield 4f orbitals of Er^{3+} in compound semiconductors from first-order host lattice effects; likewise, a similar transition has been observed in glass.[11] This opens up exciting possibilities for creating optical devices in silicon and integrating electrical and optical devices with Si-based circuits. In this way, the mature manufacturing technology of silicon can be extended to optical communications.

Ion implantation has been used to dope erbium into single-crystal silicon for optoelectronic applications; however, an efficient, room-temperature, infrared (IR) LED has not yet been demonstrated.[12] Recent measurements have suggested that the solubility of Er in Si is $1.3 \times 10^{18}/cm^3$ at 900°C. Precipitates take the form of platelets of erbium silicide 100 to 300Å in diameter and 10Å thick. Figure 2 shows the precipitate density of Si:Er for a 900°C anneal versus concentration of Er. The photoluminescence (PL) saturates at $5 \times 10^{17}/cm^3$, below the apparent solubility limit.[13] Researchers have applied a variety of methods to increase the solubility or optical efficiency of erbium in silicon. For example, Polman *et al.*[14] reported that the solubility of Er can be increased if Si is amorphized before Er implantation. Several papers[14-18] have

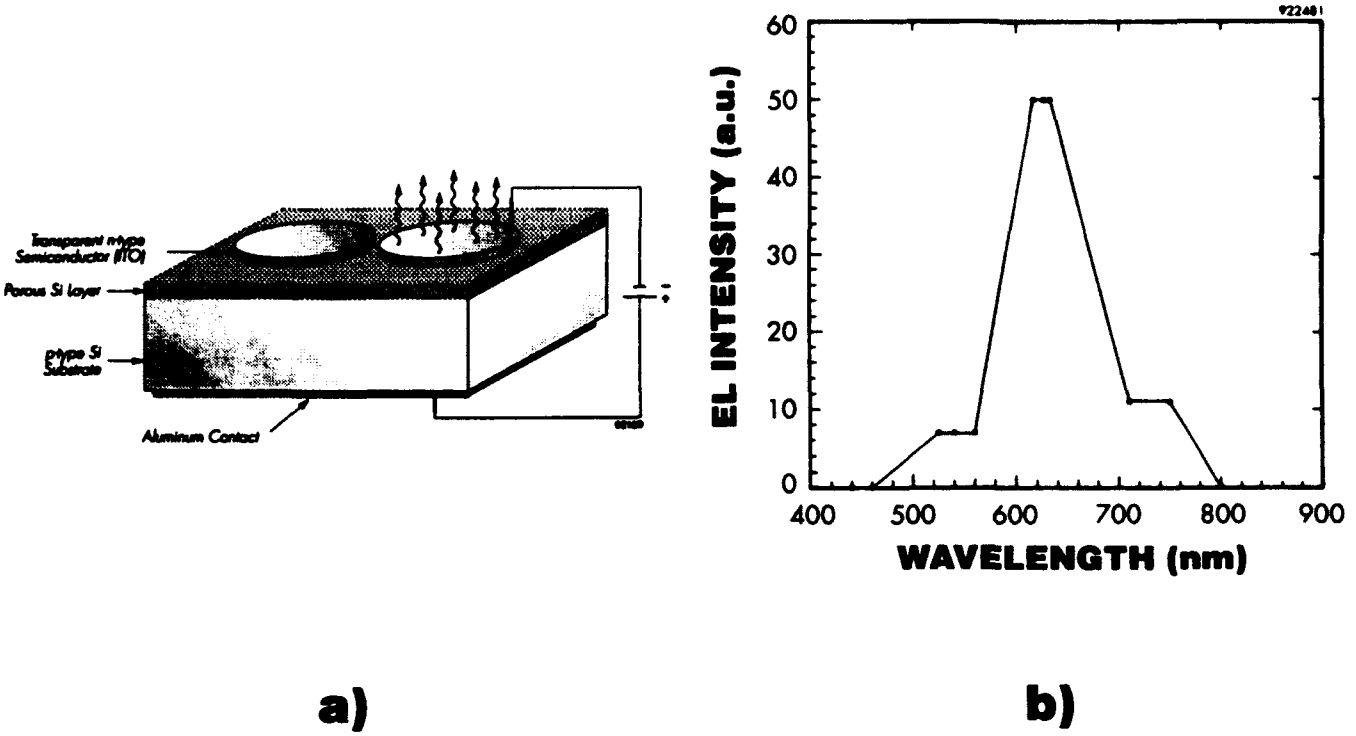

Figure 1 *a) Schematic structure and b) EL spectrum of the PSL/ITO heterojunction LEDs.*

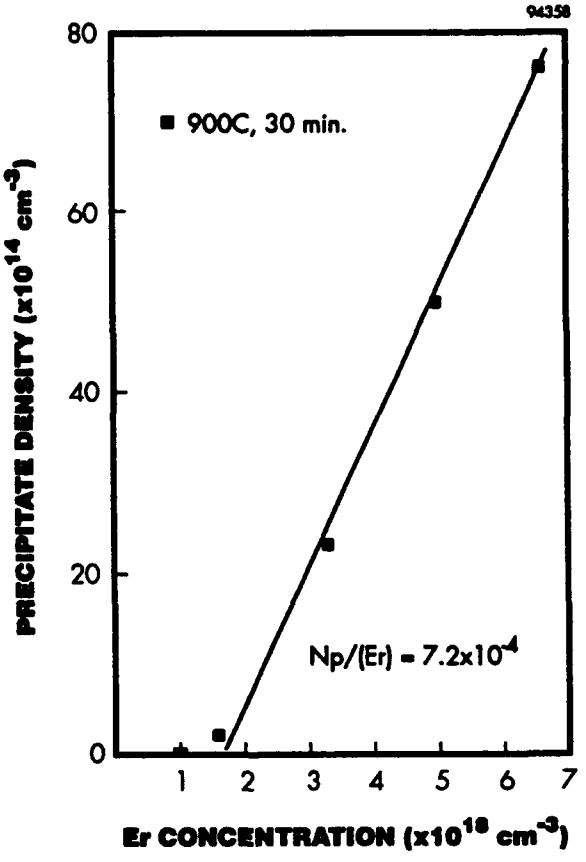

Figure 2 *Precipitate density versus Er peak concentration for Si:Er annealed at 900°C.*[13]

indicated that, after introducing oxygen or other impurities, the light emission of Er-implanted Si is enhanced. Indeed, recent results of Er-implanted silicon measured with extended X-ray absorption fine-structure (EXAFS) show Er-implanted, Czochralski-grown silicon (CZ-Si) involves a sixfold bonding of erbium to oxygen impurity atoms and forms an optically-active species. In contrast, erbium-implanted, float-zone silicon (FZ-Si), which contains far less oxygen, results in a twelvefold bonding of erbium to silicon, yielding an optically-inactive species, as shown in Figure 3.[17]

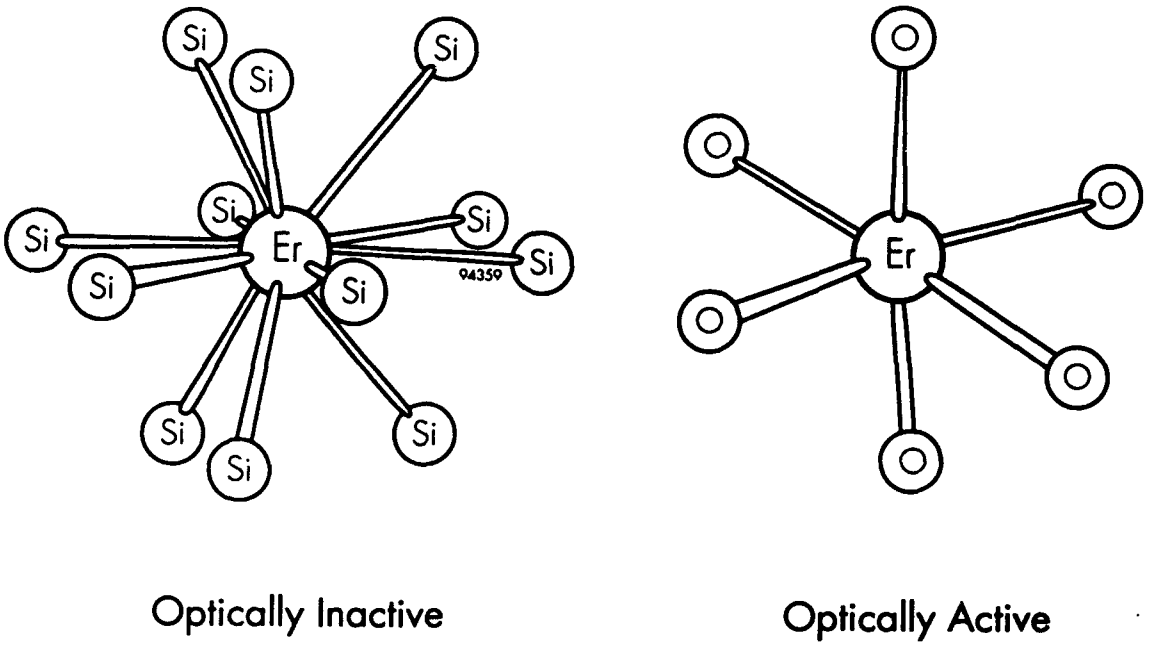

Figure 3 *Schematic picture of first coordination shell surrounding Er in FZ-Si (left) and CZ-Si (right). Erbium in CZ-Si, which is optically active, has a sixfold coordination of oxygen atoms at an average distance of 2.25Å. In contrast, erbium in FZ-Si, which is optically inactive, is coordinated to twelve Si atoms at a mean distance of 3Å.*[17]

Based on the published literature for Er-implanted Si,[14-18] one can infer that optical inefficiency is predominantly caused by erbium's limited solubility in silicon (which is influenced by the recrystallization process) and by a dependence on the presence of oxygen. We anticipate that porous silicon will prove to be an excellent host for rare earth elements because:

- recovery of damage resulting from implantation into Si nanostructures should occur at much lower annealing temperatures than in bulk Si. Defects such as vacancies or interstitials created by Er implantation need only travel a relatively small distance to reach the free surface (sink) as compared to MeV implantation into bulk Si where defects must travel rather long distances (several hundred/thousand angstroms) to reach the sink. Annealing at 900°C or higher is used to recrystallize bulk Si; however, this high temperature could result in formation of silicides rather than erbium with oxygen coordination.

- Erbium in the silicon nanostructures can easily acquire oxygen because the surface area of the nanostructures is enormous and the average distance between the erbium and surface oxygen is on the order of a few nanometers.

- In contrast to Er in bulk Si, Er in porous Si does not precipitate because porous Si consists of free-standing, quantum-confined structures with distinct physical boundaries, as shown in Figure 4.

- Porous Si has a higher bandgap (1.8 to 2.0 eV) (see Figure 5) than bulk Si (1.1 eV); thus stronger IR emission and weaker temperature dependence are expected, as shown in Figure 6.[15]

- Spire has demonstrated (see Figure 1) fabrication of the first yellow- and orange-emitting heterojunction light-emitting diodes (LEDs) based on silicon, and details can be found in our U.S. Patent entitled "Optoelectronic Switching and Display Device with Porous Silicon."[7] We believe that an infrared LED based on rare earth doped silicon is a practical expectation. Details and theory of energy band quantum confinement silicon LEDs have been given in several publications. Spire's results have achieved nationwide media attention through reports in a number of magazines and newspapers, including The Wall Street Journal (December 6, 1991, p. B3), Scientific American (March 1992, p. 102), Lasers & Optronics (January 1992 , p. 8), and The Electronics Engineering Times (May 25, 1992, p. 4).

94376

Figure 4 *Cross-sectional TEM micrograph of Spire's working np-heterojunction porous silicon LED, showing the silicon wire structures underneath ITO.*

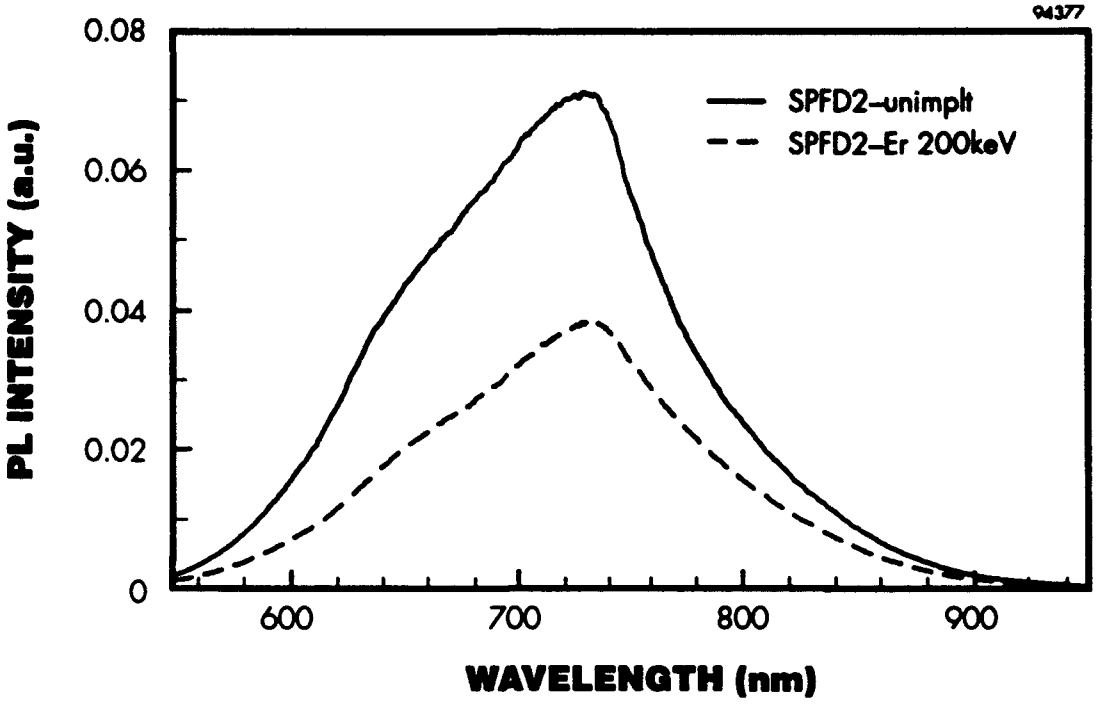

Figure 5 *Visible PL spectra of porous Si samples before and after implantation with a dose of 10^{15} Er^{+}/cm^{2} at 190 keV. See Figure 13 IR PL emission spectra.*

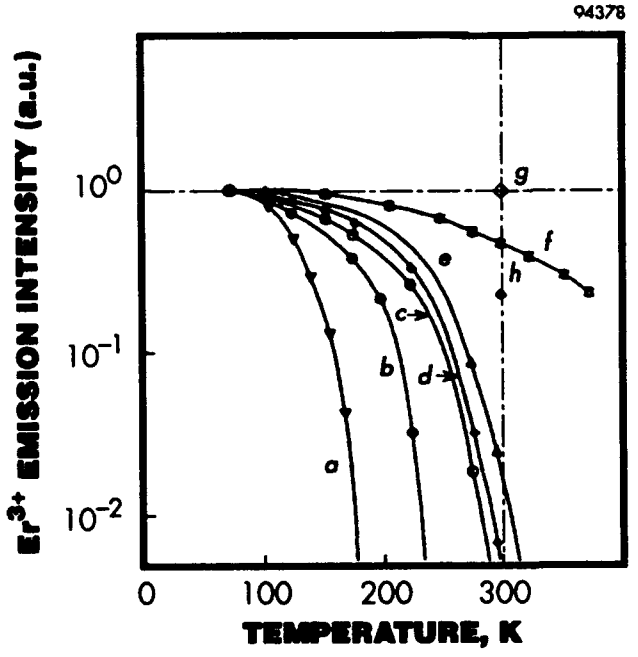

(a) $Ga_{0.38}In_{0.62}As_{0.84}P_{0.12}$ (E_G = 0.807 eV)
(b) Si (E_G = 1.12 eV)
(c) InP (E_G = 1.27 eV)
(d) GaAs (E_G = 1.43 eV)
(e) $Al_{0.17}Ga_{0.83}As$ (E_G = 1.67 eV)
(f) ZnTe (E_G = 2.26 eV)
(g) CdS (E_G = 2.42 eV)
(h) a – Si : H (E_G = 1.8 eV)

Figure 6 *Er^{3+} emission intensity as a function of temperature for various semiconductor hosts.*[15]

SECTION 2

PHASE I TECHNICAL OBJECTIVES

Standard InGaAsP IR LEDs find limited use because of their very broad emission spectra (see Figure 7), which tend to distort data transmitted in fibers. This distortion of transmitted signals is the result of chromatic dispersion, which originates from wavelength dependence on the index of refraction. The problem becomes further amplified because of the dependence of the width of emission spectra of InGaAsP LEDs on operating temperature and power. In contrast, the luminescence peak from Er is narrow because of its atomic level transitions and Er doped in porous Si has excellent temperature stability.

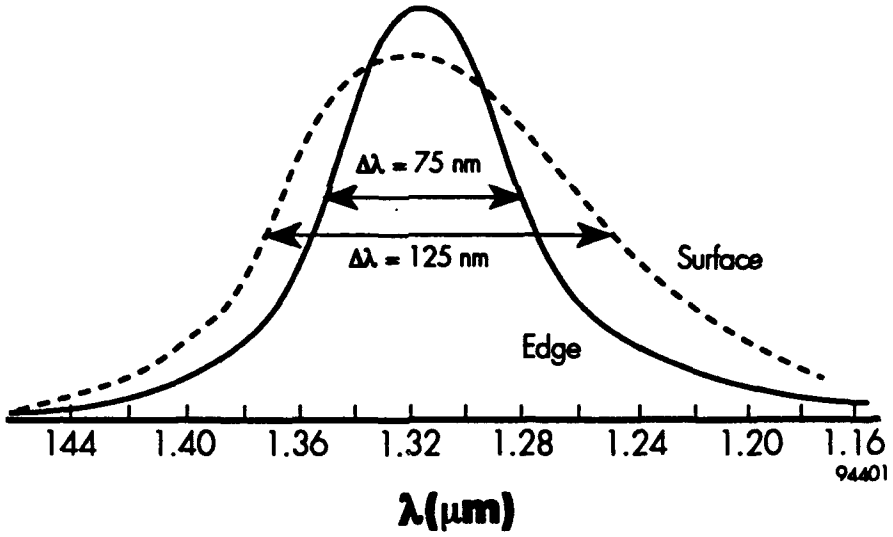

Figure 7 *Spectral output curve for InGaAsP surface- and edge-emitting LEDs.*[19]

The objective of Phase I work was to demonstrate a strong room-temperature emission at 1.54 μm from Er embedded in porous Si. As we have shown in this report, we have achieved our objective and observed infrared emission from Er-doped porous silicon which is comparable to that of InGaAs material typically employed in commercial infrared light-emitting diodes. Porous silicon doped with erbium is a low-cost alternative which can be easily integrated with standard silicon wafer technology.

SECTION 3
PHASE I TECHNICAL APPROACH AND EXPERIMENTAL RESULTS

3.1 EXPERIMENTAL PROCEDURE

3.1.1 Formation of Porous Silicon Layers

We anodically etched a large number of p-type crystalline Si wafers with (100) orientations to form porous Si surface layers. Figure 8 shows the anodic etching system that was used for producing porous Si samples. This system relies on a Keithley Model 225 current source, with the sample connected as the anode (+) and a foil platinum as the cathode (-). The electrolyte, usually a 1:1 mixture of hydrofluoric acid (HF) and ethanol, is contained in a teflon vessel. The silicon wafers are held in a specially prepared jig which exposes only the front surface to the solution, allowing the electrical contact on the back to be isolated from any liquid. The silicon samples were carefully etched in the HF solution using current densities between 10 mA/cm^2 and 100 mA/cm^2.

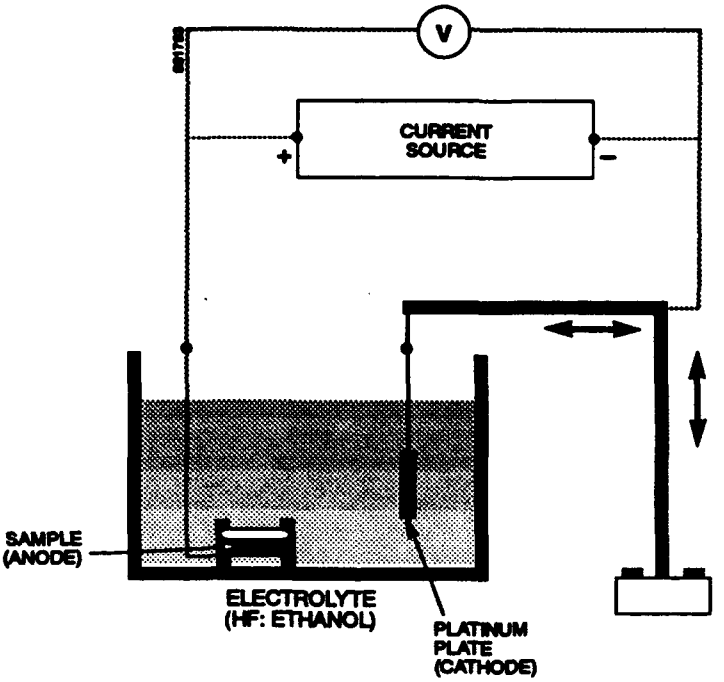

Figure 8 *Schematic diagram of the anodic etching system used at Spire for fabricating porous silicon samples.*

3.1.2 Erbium Implantation and Annealing

We used an in-house ion implanter to implant erbium ions into various substrates with doses ranging from 10^{14} to 10^{16}/cm^2 at energies between 50 and 400 keV. Figure 9 shows one of Spire's ion implanters. Samples were then annealed using an in-house furnace in order to recrystallize the damaged porous Si and activate the dopant. The samples were annealed in a nitrogen ambient at temperatures ranging from 500 to 850°C for periods between 15 and 120 minutes.

a)

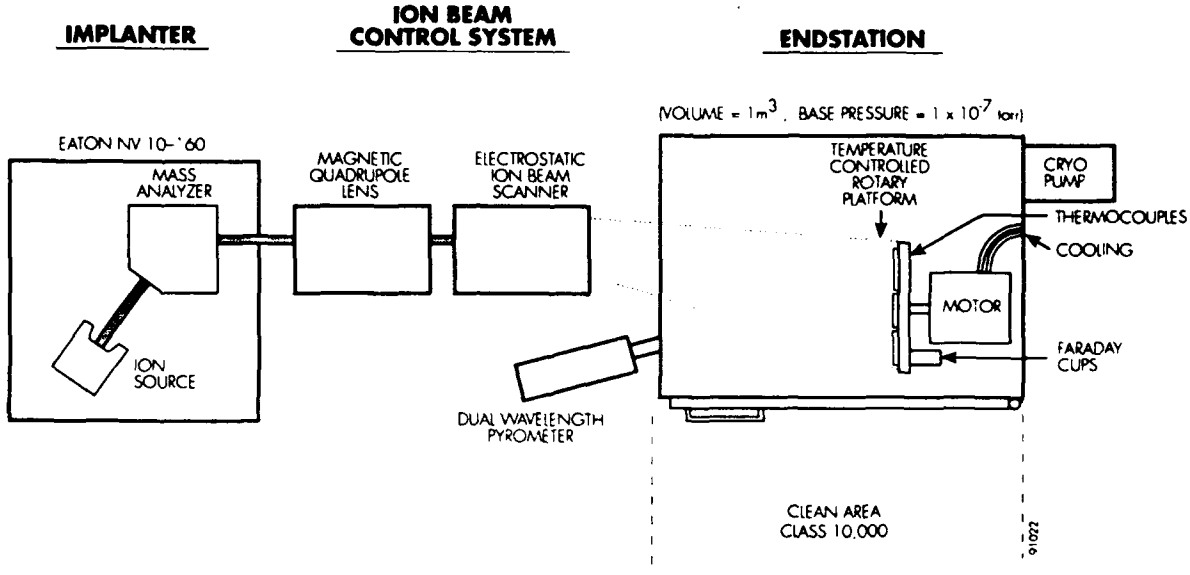

b)

Figure 9 *a) Spire's ion implanter for high-dose implantation, and b) schematic of ion implanter beam transport.*

3.1.3 Material Characterization

RBS/channeling was employed to measure layer thicknesses and determine the erbium concentration profile in porous and bulk Si. The structures of selected samples were analyzed using cross-sectional transmission electron microscopy (XTEM).

3.1.4 Optical Characterization

3.1.4.1 Visible PL

Visible photoluminescence (PL) measurements were carried out from 0.5 to 0.95 μm. Excitation was created by a Coherent INNOVA 60 argon laser using the 488 nm beam. The emission was dispersed by a SPEX Model 1702/04 grating monochromator and observed by a Si detector. An EG&G Model 5207 lock-in amplifier interfaced to a Hewlett-Packard Model 86B computer collected the data.

3.1.4.2 Infrared PL

Infrared measurements were carried out in collaboration with Professor Clive H. Perry and Dr. Feng Lu of Northeastern University. The IR PL was excited by a Coherent INNOVA 70 argon laser, and measurements were carried out at laser powers between 10 and 450 mW. An interference band-pass filter was placed in front of the samples to eliminate plasma lines from the laser beam. The samples were illuminated from the porous Si side and IR PL was collected at a near-backscattering geometry. A SPEX 1401 0.75m double monochromator equipped with a pair of 600 line/mm gratings was utilized for the IR PL studies. The PL signal was detected by a liquid nitrogen cooled NorthCoast Ge detector. A thin GaAs wafer polished on both sides was placed in front of the collecting lens of the detector to filter lines from the second- and third-order grating scattering. Both entrance and exit slits of the monochromator were set at 1000 μm, resulting in a spectral resolution of ~1 nm, which was much smaller than the Er peak widths (≥ 7 nm) observed from the samples.

3.2 EXPERIMENTAL RESULTS

3.2.1 Concentration Profile of Implanted Erbium

Most published literature on IR PL of Er:Si reports using bulk Si samples implanted with erbium at the MeV range.[20] One of the aims of our work was to produce samples for efficient optical communication using commercial ion implanters. From an economical point of view, implantation in the MeV range poses several problems. First of all, the initial investment cost of implanters is related exponentially to the energy output. Secondly, the operation and maintenance of these machines is much more complicated, and typical high-energy implanters deliver less current (beam).

Figure 10 shows RBS spectra of bulk Si and porous Si implanted with a dose of 10^{15} Er^+/cm^2 at 190 keV. Figure 11 shows a concentration profile of Er implanted into porous Si before and after annealing at 650°C, indicating that no redistribution of Er has occurred. Erbium is distributed in a region less than 2000Å from the surface. Er peak concentration is about 0.3%, which corresponds to $1.5 \times 10^{20}/cm^3$. Figure 12 is a comparison of simulated profiles for a porous Si sample implanted at 190 keV and 4.5 MeV with a dose of 10^{15} Er/cm^2. In Figure 13 we compare RBS data for samples implanted at 50, 200, and 400 keV.

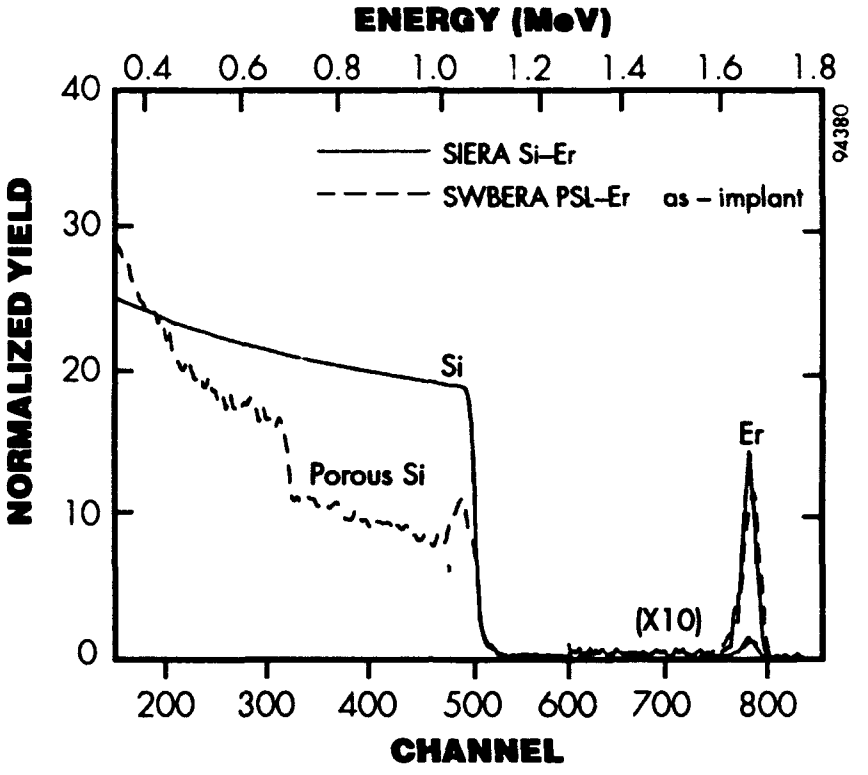

Figure 10 *RBS spectra of bulk Si and porous Si implanted with a dose of 10^{15} Er^{+}/cm^{2} at 190 keV.*

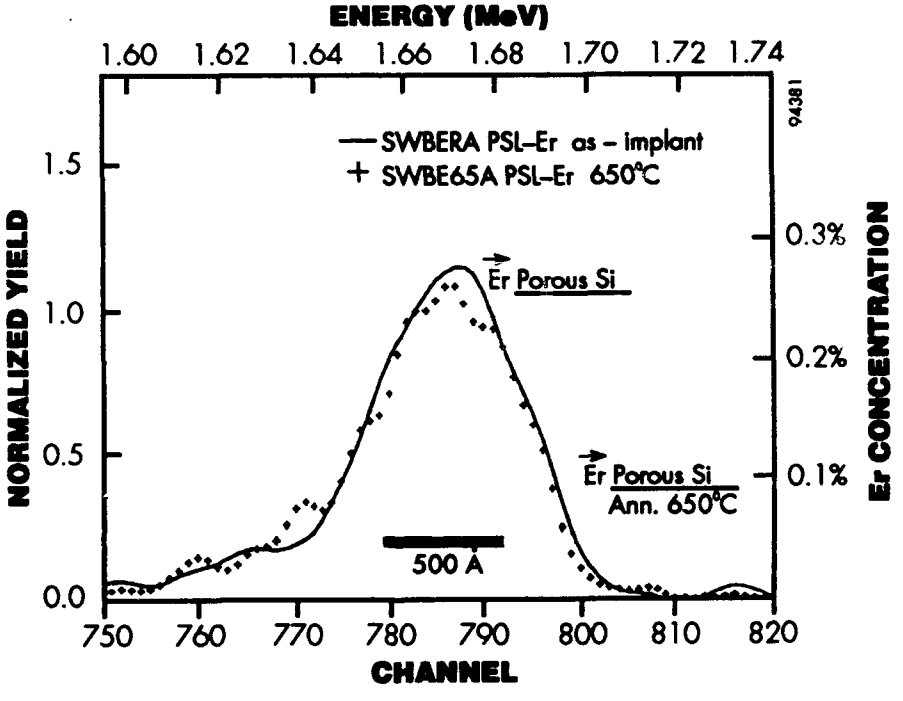

Figure 11 *Comparison of concentration depth profiles of an Er-implanted porous Si sample a) before annealing and b) after annealing at 650°C, indicating that no substantial redistribution of Er occurs after annealing at 650°C.*

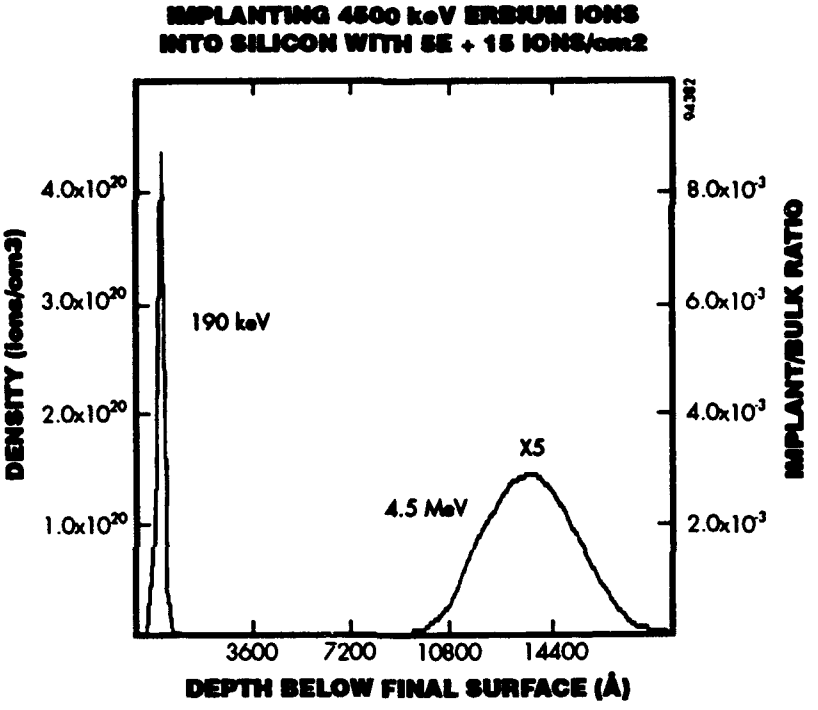

Figure 12 *Computer simulation of Er implantation at 190 keV and at 4.5 MeV. Note that peak concentration for erbium implanted at 190 keV is about $10^{20}/cm^3$, as compared to that for erbium implanted at 4.5 MeV, which is only about 10^{18} cm^3.*

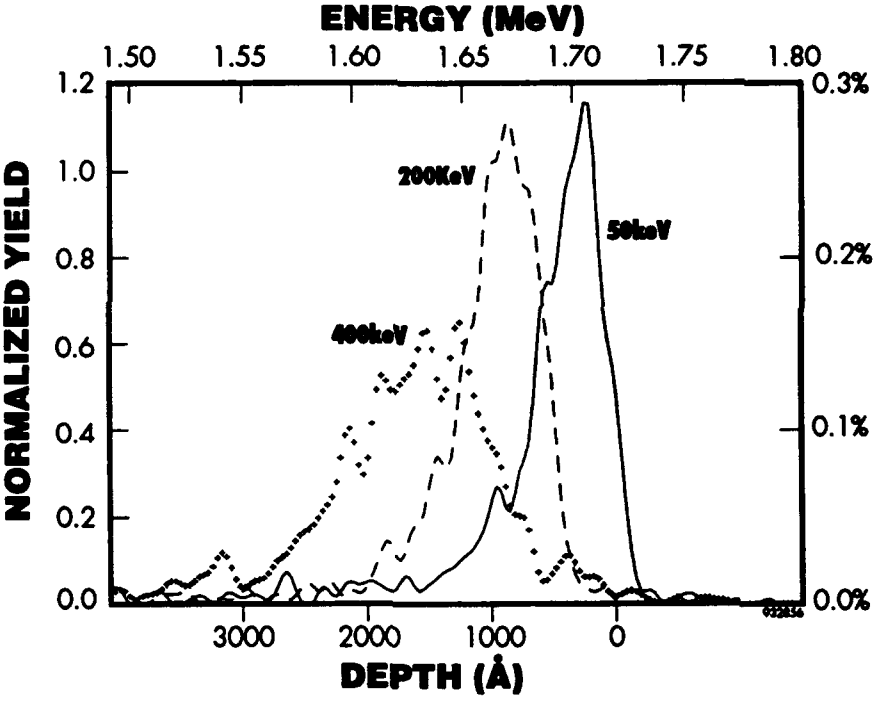

Figure 13 *Concentration depth profile, as determined by RBS measurements, of Er implanted with a dose of $10^{15}/cm^2$ at 50, 200, and 400 keV into porous Si.*

3.2.2 Visible PL

We have measured the visible PL of unimplanted and Er-implanted porous Si, typical results for Er implanted with a dose of $10^{15}/cm^2$ at 190 keV are shown in Figure 5. Comparison of these two spectra indicates that after Er implantation, the intensity of visible PL has been reduced by a factor of approximately two.

3.2.3 Comparison of IR PL Spectra for Er Implanted into Porous Si with Bulk Si and GeSi

Figure 14 compares room-temperature IR PL spectra from erbium implanted into bulk Si, and porous Si at 190 keV with a dose of $10^{15}/cm^2$ and annealed at 650°C for 30 minutes in N_2. Er-implanted porous Si shows a strong IR emission which consists of double peaks at 1.535 μm and 1.550 μm with a full width at half maximum (FWHM) of ~11 and ~9 nm, respectively. This spectrum is identical to the EL spectra measured at 100K (as shown in Figure 15) of a silicon substrate implanted with erbium at 4.5 MeV and co-implanted with oxygen.[20] No IR emission was observed for any Er-implanted bulk Si samples, even at 9K.

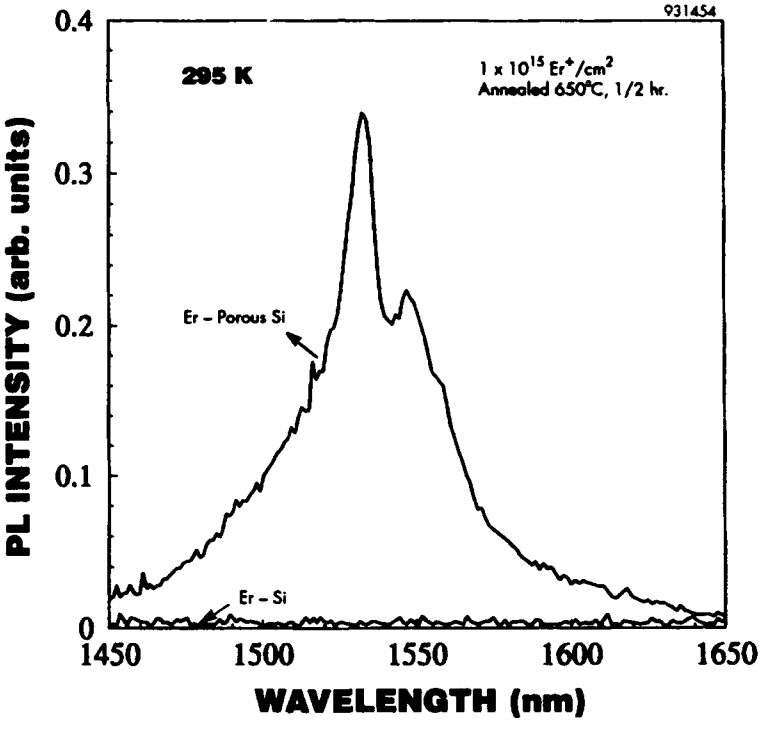

Figure 14 *Room-temperature IR emission from Er implanted into porous Si and bulk Si with a dose of $10^{15}/cm^2$ and annealed at 650°C. No PL was observed for Er implanted into GeSi or bulk Si. (See Figure 5 for visible PL and Figure 11 for Er profile.)*

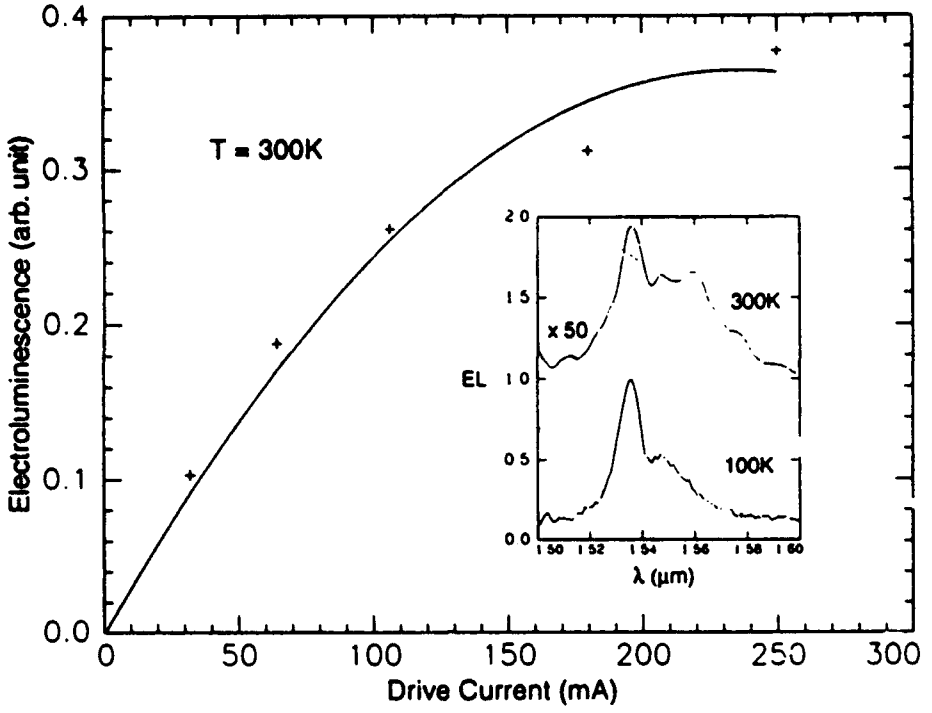

Figure 15 *Si:Er LED intensity as a function of drive current. The inset shows the EL spectra at 100K and 300K.*[20]

3.2.4 Comparison of IR PL from Er in Porous Si and in Quartz

Strong IR PL was observed from Er-implanted with a dose of 10^{15} Er^+/cm^2 at 200 keV and annealed at 650°C. No luminescence peak was observed from the quartz sample under the same conditions. Figure 16 shows weak room-temperature IR emission from a quartz implanted with a dose of 10^{15} Er^+/cm^2 at 400 keV and annealed at 900°C. Figure 17 shows PL measured at 9K for the latter sample. A comparison of results from Er implanted into porous Si and into quartz clearly indicates that the Er in porous Si is not located in an SiO_2 environment.

3.2.5 Comparison of Er in Porous Si with $In_{0.53}Ga_{0.47}As$

To determine the relative PL intensity of Er embedded in Si nanostructures, it is important to compare the PL of Er-implanted porous Si to a well-defined reference. Since standards have not yet been established, we have compared our IR PL emission from Er in porous Si with a highly doped $In_{0.53}Ga_{0.47}As$ film grown on InP. $In_{0.53}Ga_{0.47}As$ is a direct-bandgap material which is used for room-temperature commercial infrared LEDs. As shown in Figure 18, the intensity of IR emission at 1.54 μm for Er in porous Si is approximately 8% of $In_{0.53}Ga_{0.47}As$.

3.2.6 Effects of Annealing Temperature on Efficiency of IR Emission

We have carried out a systematic study to determine the efficiency of IR emission as a function of annealing temperature. Figure 19 shows room-temperature PL intensity of an Er-implanted (10^{15} Er^+/cm^2 at 190 keV), annealed porous Si sample (SW32B-Er). Annealing was

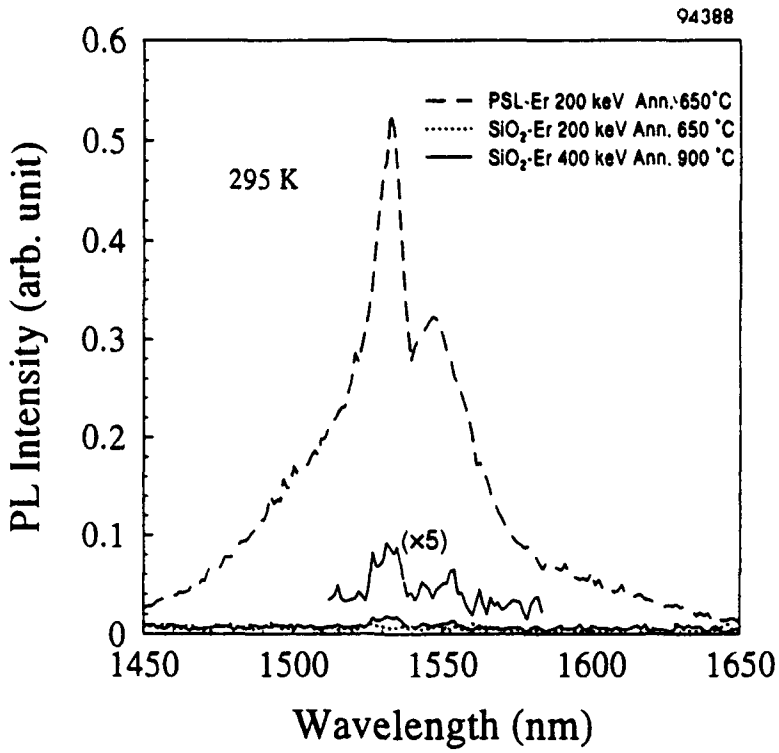

Figure 16 *Room-temperature PL spectra of Er implanted with a dose of 10^{15} Er^+/cm^2 into porous Si at 200 keV, and into quartz at 200 and 400 keV. Strong IR emission was observed for the porous Si after annealing at 650°C. In contrast, no IR emission was observed for quartz processed under similar conditions. However, weak luminescence was observed from quartz when implanted at 400 keV and annealed at 900°C (see Figure 17).*

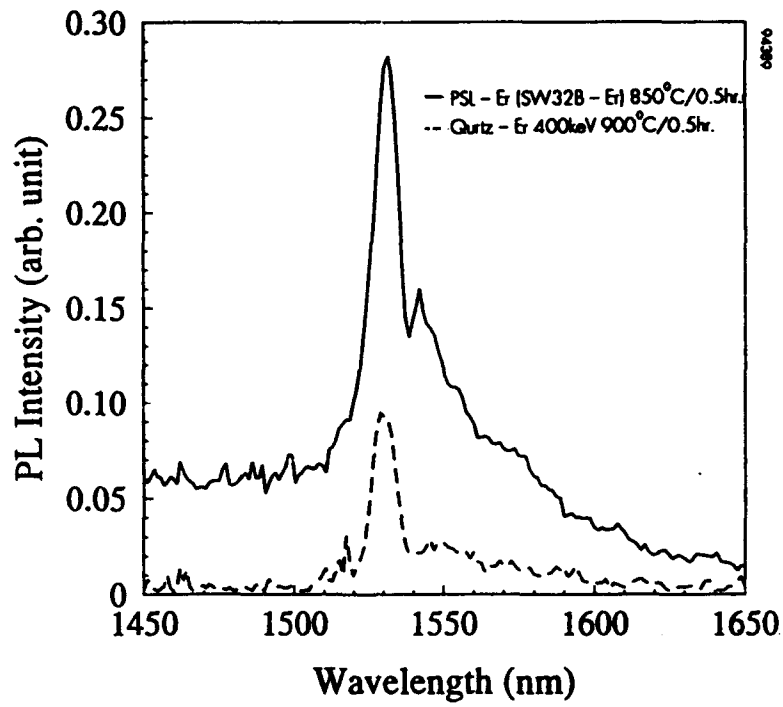

Figure 17 *IR PL spectra measured at 9K of porous Si and quartz samples (see Figure 16).*

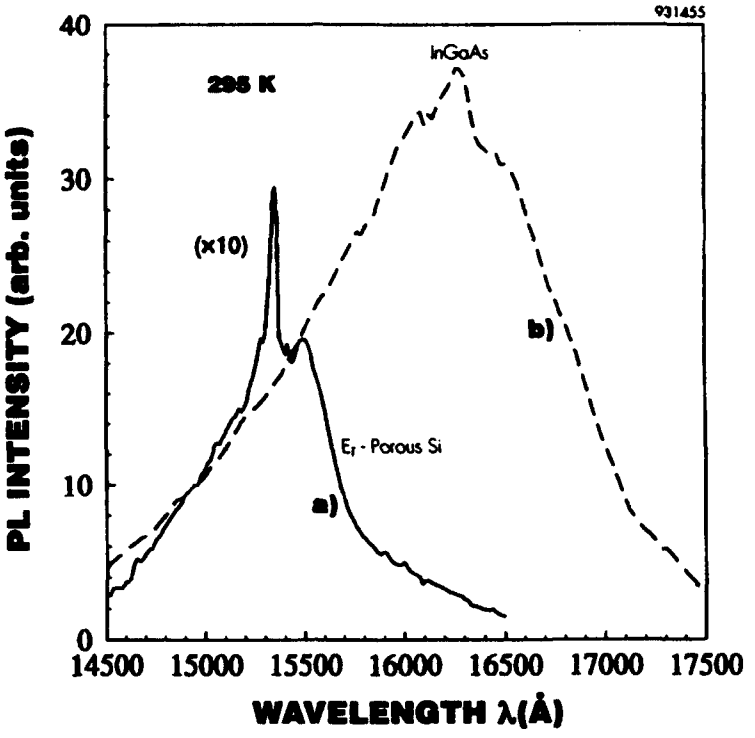

Figure 18 *Room-temperature IR PL spectra from a 2 μm highly-doped $In_{0.53}Ga_{0.47}As$ film on InP and a porous Si sample implanted with a dose of 10^{15} Er^+/cm^2 at 190 keV.*

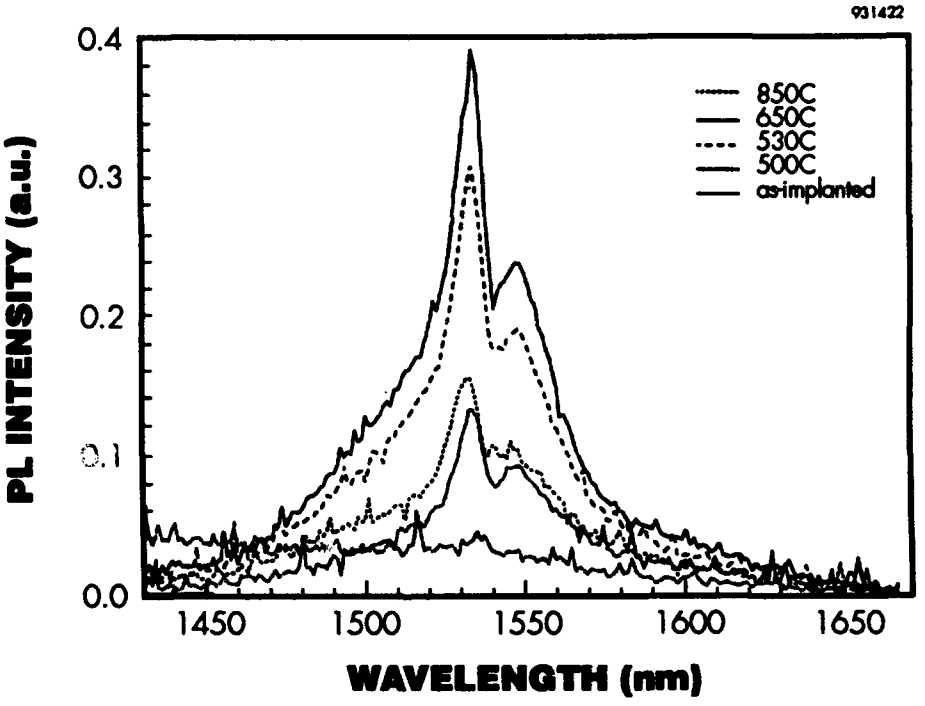

Figure 19 *PL spectra of porous Si implanted with a dose of 10^{15} Er^+/cm^2 at 190 keV and annealed at temperatures between 500 and 850°C.*

carried out in N_2 for 30 minutes at temperatures between 500 and 850°C. The intensity of the PL increased with annealing temperature and peaked at 650°C; however, annealing at temperatures above 650°C resulted in a decrease in PL intensity. It is known that the most efficient PL from Er in bulk Si is obtained by annealing at 900°C. In comparison, porous Si shows an optimum PL efficiency at an annealing temperature of 650°C. Figure 20 shows PL intensity as a function of anneal temperature for an Er-implanted porous Si sample.

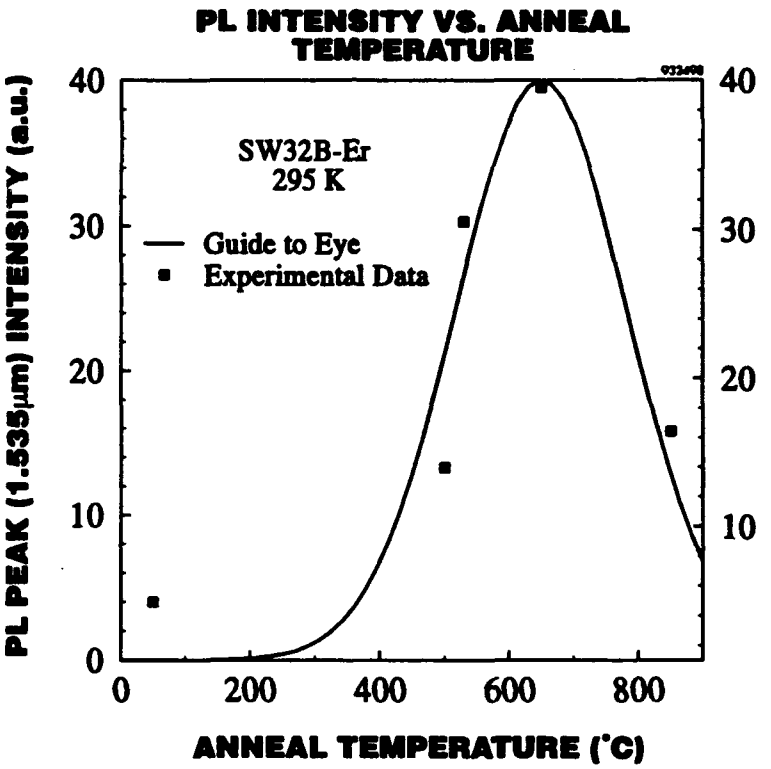

Figure 20 *PL intensity as a function of anneal temperature for an Er-implanted porous Si sample. Note that the maximum PL efficiency occurs for annealing at 650°C.*

3.2.7 Temperature Dependence of Er in Porous Si

The strong temperature dependence of PL intensity for Er-doped bulk Si is one of the major obstacles preventing the application of Si:Er in optoelectronics.[21] Luminescence from Er in crystalline Si typically decreases 1000 times once the temperature increases from 77K to room temperature. We have studied the temperature dependence of PL intensity in Er-implanted porous Si from 10K to room temperature. Figure 21 shows IR spectra measured at 10, 80, and 295K. Figure 22 compares our results of Er in porous Si measured at different temperatures with the most recent work by Priolo *et al.*, which shows the results for Er implanted into Si in the energy range from 0.5 to 5.0 MeV, with and without co-doping with oxygen implanted from 0.15 to 1.4 MeV.[21] Figure 21 clearly demonstrates a very weak temperature dependence, less than a factor of two from 10K to room temperature for Er implanted in porous Si.

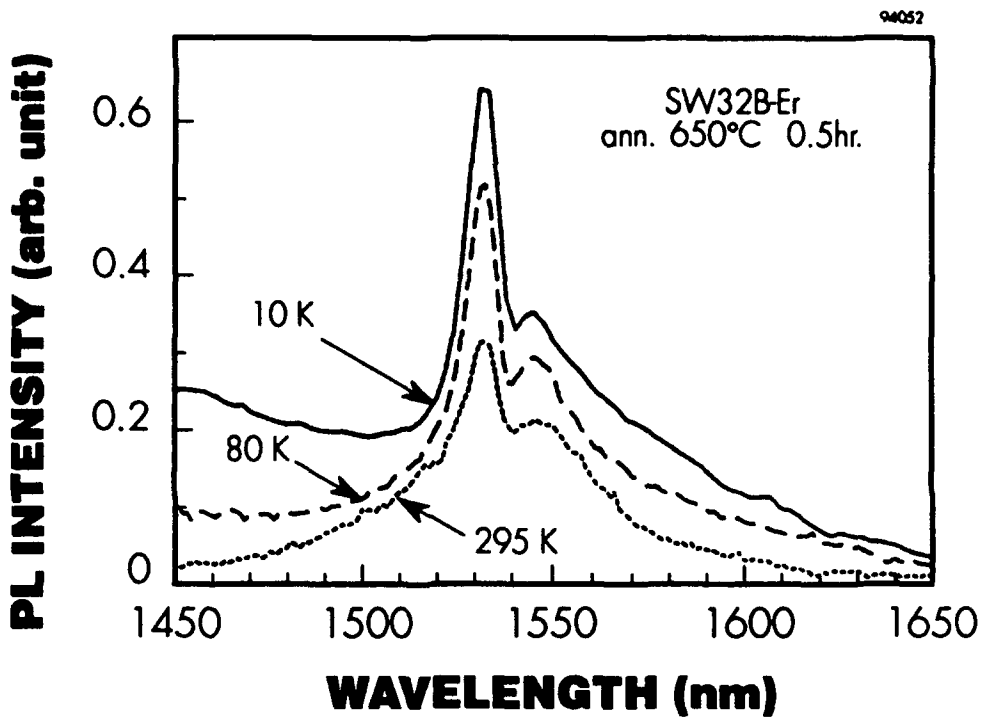

Figure 21 *IR spectra measured at 10K, 80K, and 295K for Er-implanted porous Si.*

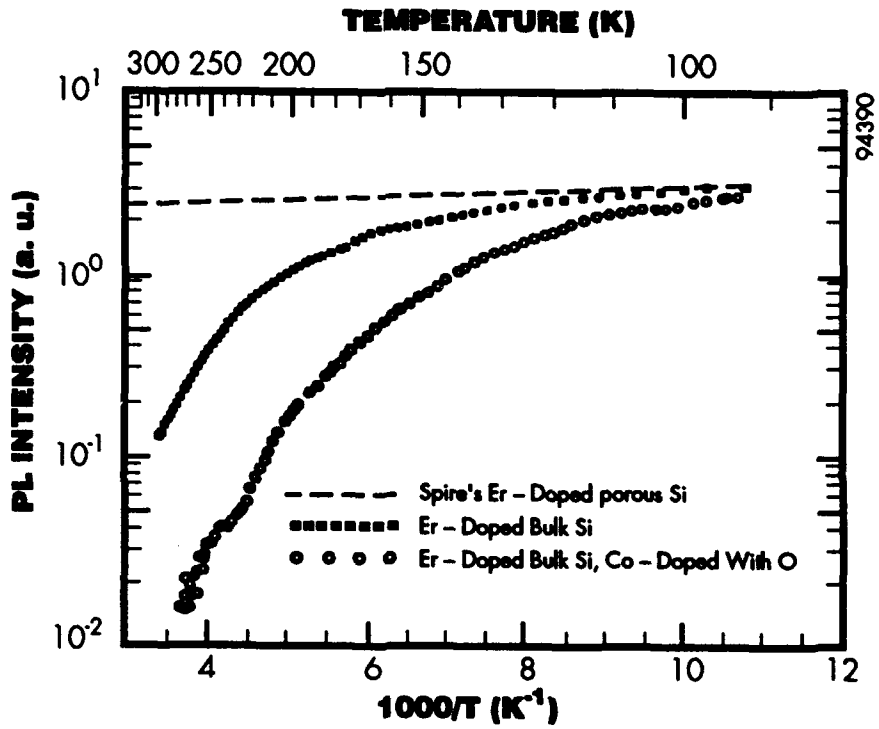

Figure 22 *Temperature dependence of PL intensity for a) Er implanted into porous Si at 190 keV and annealed at 650°C; b) Er implanted into Bulk Si in the range from 0.5 to 5.0 MeV; and, c) Er implanted into bulk Si and co-implanted with oxygen from 0.15 to 1.4 MeV.*

SECTION 4

CONCLUSIONS AND RECOMMENDATIONS

Phase I results showed the first strong, room-temperature, infrared emission from Er-implanted porous silicon. This emission consisted of double peaks at 1.535 and 1.550 μm and had an FWHM of ~11 and ~9 nm, respectively. This spectrum is identical to the EL spectra (measured at 100K) of a silicon substrate implanted with erbium at 4.5 MeV and co-implanted with oxygen.[20]

We implanted erbium into porous Si, bulk Si, GeSi, quartz, and sapphire with a dose of $10^{15}/cm^2$ at energies ranging from 50 to 400 keV. Samples were then annealed for 30 minutes in nitrogen at temperatures ranging from 500°C to 900°C. The highest emission intensity was observed for samples which had a peak concentration of 1.5 x 10^{20} Er/cm^3 and had been implanted at energies as low as 190 keV and annealed at 650°C. However, no IR emission was observed from Er in bulk Si, GeSi, quartz, and sapphire which had been implanted and annealed under these conditions. We observed very weak room-temperature IR emission from quartz implanted with a dose of 10^{15} Er^+/cm^2 at 400 keV and annealed at 900°C, which is 100 to 1000 times weaker than that observed for Er implanted at 190 keV into porous Si. These results indicate that strong emission is due to Er in quantum-confined Si nanostructures and not from Er in SiO_2 or in Si with bulk properties.

A systematic study to determine the intensity of IR emission as a function of annealing temperature shows that the PL intensity increased with annealing temperature and peaked at 650°C and that annealing at temperatures above 650°C resulted in a decrease in PL intensity. The temperature dependence of PL intensity for Er-doped Si is one of the major obstacles preventing the application of Si:Er in optoelectronics. Luminescence from Er in crystalline Si typically decreases 1000 times once the temperature increases from 77K to room temperature. However, we have shown that the temperature dependence of Er in porous Si is less than a factor of two in this temperature range.

We compared our IR PL emission from Er in porous Si with a highly doped $In_{0.53}Ga_{0.47}As$ film grown on InP. $In_{0.53}Ga_{0.47}As$ is a direct-bandgap material which is used in fabrication of room-temperature IR LEDs. Our results show that the emission intensity of Er in porous Si is comparable with that of $In_{0.53}Ga_{0.47}As$. Standard IR LEDs have limited use because of their very broad (100 to 200 nm) emission spectra, which tend to distort data transmitted in fibers. In contrast, we have shown that the luminescence peak from erbium is narrow and possesses very good temperature stability. Based on related porous silicon work at Spire, as well as results obtained from the present work, we believe that porous silicon doped with erbium can be a practical and low-cost alternative which can be easily integrated with advanced silicon wafer technology.

In Phase II, we will carry out a systematic study in order to understand the mechanism involved in light emission from Er in porous Si and optimize the processes to enhance its light efficiency. However, emphasis will be placed on fabrication of light-emitting devices. In Phase II, we will fabricate two types of EL devices: those operating based on injection-induced luminescence (LEDs), and those operating based on impact-excited luminescence.

SECTION 5

REFERENCES

1. L.T. Canham, *Appl. Phys. Lett.* **57**, 1046 (1990).
2. R.L. Smith and S.D. Collins, *J. Appl. Phys.* **71**, R1 (1992).
3. F. Namavar, P. Maruska, and N.M. Kalkhoran, *Appl. Phys. Lett.* **60**, 2514 (1992).
4. A. Richter, W. Lang, P. Steiner, F. Lozlowski, and H. Sandmeier, *Mat. Res. Soc. Symp. Proc.* **246**, 209 (1991).
5. N. Koshida and M. Katsuno, *Appl. Phys. Lett.* **60**, 347 (1992).
6. T. Futagi, T. Matsumoto, M. Katsuno, Y. Ohta, H. Mimura, and K. Kitamura, *Mat. Res. Soc. Symp. Proc.* **283**, 389 (1993).
7. F. Namavar, N.M. Kalkhoran, and H.P. Maruska, U.S. Patent No. 5,272,355 (December 21, 1993).
8. H. Ennen, J. Schneider, G. Pomrenke, and A. Axmann, *Appl. Phys. Lett.* **43**, 943 (1983).
9. H. Ennen, G. Pomrenke, A. Axmann, K. Eisele, W. Haydl, and J. Schneider, *Appl. Phys. Lett.* **46**, 381 (1985).
10. G.S.Pomrenke, H. Ennen, and W. Haydl, *J. Appl. Phys.* **59**, 601 (1986).
11. A. Polman, D.C. Jacobson, D.J. Eaglesham, R.C. Kistler, and J.M. Poate, *J. Appl. Phys.* **70**, 3778 (1991).
12. Y.-H. Xie, E.A. Fitzgerald, and Y.J. Mii, *J. Appl. Phys.* **70**, 3223 (1991).
13. D.J. Eaglesham, J. Michel, E.A. Fitzgerald, D.C. Jacobson, J.M. Poate, J.L. Benton, A. Polman, Y.-H. Xie, and L.C. Kimerling, *Appl. Phys. Lett.* **58**, 2797 (1991).
14. A. Polman, J.S. Custer, E. Snoeks, and G.N. van den Hoven, *Appl. Phys. Lett.* **62**, 507 (1993).
15. P.N. Favennec, H. L'Haridon, D. Moutonnet, M. Salvi, and M. Gauneau, *Mat. Res. Soc. Symp. Proc.* **301**, 181 (1993).
16. J. Michel, L.C. Kimerling, J.L. Benton, D.J. Eaglesham, E.A. Fitzgerald, D.C. Jacobson, J.M. Poate, and R.F. Ferrante, *Mat. Sci. Forum* **83-87**, 653-658 (1992).
17. D.L. Adler, D.C. Jacobson, D.J. Eaglesham, M.A. Marcus, J.L. Benton, J.M. Poate, and P.H. Citrin, *Appl. Phys. Lett.* **61**, 2181 (1992).
18. J. Michel, J.L. Benton, R.F. Ferrante, D.C. Jacobson, D.J. Eaglesham, E.A. Fitzgerald, Y.-H. Xie, J.M. Poate, and L.C. Kimerling, *J. Appl. Phys.* **70**, 2672 (1991).
19. T.P. Lee, C.A. Burros, Jr., R.H. Saul, *Optical Fiber Telecommun. II* **12**, 467, (1988).
20. F.Y.G. Ren, J. Michel, Q. Sun-Paduano, B. Zheng, H. Kitagawa, D.C. Jacobson, J.M. Poate, and L.C. Kimerling, *Mat. Res. Soc. Symp. Proc.* **301**, 87 (1993).
21. F. Priolo, G. Franzó, S. Coffa, A. Polman, V. Bellani, A. Carnera, and C. Spinella, *Mat. Res. Soc. Symp. Proc.* **316** (1994).